Autocalibration of MEMS Accelerometers

Iuri Frosio, *Member, IEEE*, Federico Pedersini, and N. Alberto Borghese, *Member, IEEE*

Abstract—In this paper, we present a novel procedure for the on-the-field autocalibration of triaxial micro accelerometers, which requires neither any equipment nor a controlled environment and allows increasing the accuracy of this kind of microsensor. The procedure exploits the fact that, in static conditions, the modulus of the accelerometer output vector matches that of the gravity acceleration. The calibration model incorporates the bias and scale factor for each axis and the cross-axis symmetrical factors. The parameters are computed through nonlinear optimization, which is solved in a very short time. The calibration procedure was quantitatively tested by comparing the orientation produced by MEMS with that measured by a motion capture system. Results show that the MEMS output, after the calibration procedure, is far more accurate with respect to the output obtained using factory calibration data and almost one order of magnitude more accurate with respect to using traditional calibration models.

Index Terms—Accelerometer, autocalibration, microelectromechanical system (MEMS), motion capture, sensor model.

I. Introduction

THE ADVENT of microelectromechanical system (MEMS) technology has allowed miniaturized, high-performance, and cheap sensors to be built. These have found applications in many fields, ranging from pressure measurement to hard disk actuators and virtual reality [1]. MEMS accelerometers have recently been introduced to track the motion of both humans and machines [2]–[6] as they allow accurate low-budget motion capture systems to be built. This provides an alternative to costly traditional systems, which are generally based on optoelectronic technology.

Different from classical MEMS applications (for example, airbag control), where impulsive accelerations are measured, motion analysis applications require position and orientation data. To the scope, MEMS accelerometers are integrated with gyroscopes [7] or detailed models of the moving body [1], [8], and their output has to be integrated over time. The accuracy of the accelerometer output is, therefore, fundamental, and a good calibration is needed to profitably use them. The technical data reported by manufacturers are not accurate enough for this kind of application [9]; moreover, the sensor output depends on temperature and, in general, on environmental conditions [10], [11]. Therefore, they have to be calibrated in the field to obtain high accuracy [9].

We present here a novel reliable autocalibration procedure. It is based on the assumption that an inertial sensor, in static condition, is subjected only to the gravity force. As a consequence, the module of the acceleration vector measured by the sensor has to be equal to $g = 9.81$ m/s^2, independent of the sensor orientation [12], [13]. The method only requires measuring the output of the MEMS in at least nine random orientations, and it produces an accuracy of almost one order of magnitude larger compared with previously introduced techniques, like [11]. We also introduce an innovative methodology to assess the sensor accuracy based on comparing the MEMS measurements with those obtained by a motion capture system.

II. Method

A. Sensor Model

Since the adopted accelerometer is designed to provide ratiometric output [10], we consider the normalized accelerometer output $\mathbf{V^T} = [v_x, v_y, v_z]$, which is obtained by dividing the output voltage by the power supply voltage V_{CC} (that is, $v_i = V_i/V_{CC}$, for $i = x, y, z$). Let us also define the acceleration vector $\mathbf{A^T} = [a_x, a_y, a_z]$, which is expressed in the sensor local reference system $[O, X_{\mathrm{MEMS}}, Y_{\mathrm{MEMS}}, Z_{\mathrm{MEMS}})$ (Fig. 1), with the axes X_{MEMS}, Y_{MEMS} lying on the sensor surface and Z_{MEMS} orthogonal to the surface.

A mathematical model describing the accelerometer output can be described in matrix form as

$$\mathbf{A} = \mathbf{S}(\mathbf{V} - \mathbf{O}) \tag{1}$$

where

$$\mathbf{S} = \begin{bmatrix} S_{xx} & S_{xy} & S_{xz} \\ S_{yx} & S_{yy} & S_{yz} \\ S_{zx} & S_{zy} & S_{zz} \end{bmatrix}, \qquad \mathbf{O} = \begin{bmatrix} O_x \\ O_y \\ O_z \end{bmatrix} \tag{2}$$

are the scale factor matrix and the bias vector, respectively. The diagonal elements of $\mathbf{S}$ represent the scale factors along the three axes, whereas the other elements of $\mathbf{S}$ are called cross-axis factors. These terms allow describing both the axes' misalignment and the crosstalk effect between different channels caused by the sensor electronics [13]. For an ideal accelerometer, the cross-axis factors should all be equal to zero, whereas for a real one, they can be as large as 2% of the sensor sensitivity, as reported in Table I. The highest accuracy is achieved by considering the cross-axis factors in $\mathbf{S}$, as shown in Section IV. Imposing the symmetry constraint on the scale factor matrix $\mathbf{S}$ (that is, $S_{xy} = S_{yx}$, $S_{xz} = S_{zx}$, and $S_{yz} = S_{zy}$), the resulting model has nine independent parameters. Calibration consists of a procedure capable to determine these parameters.
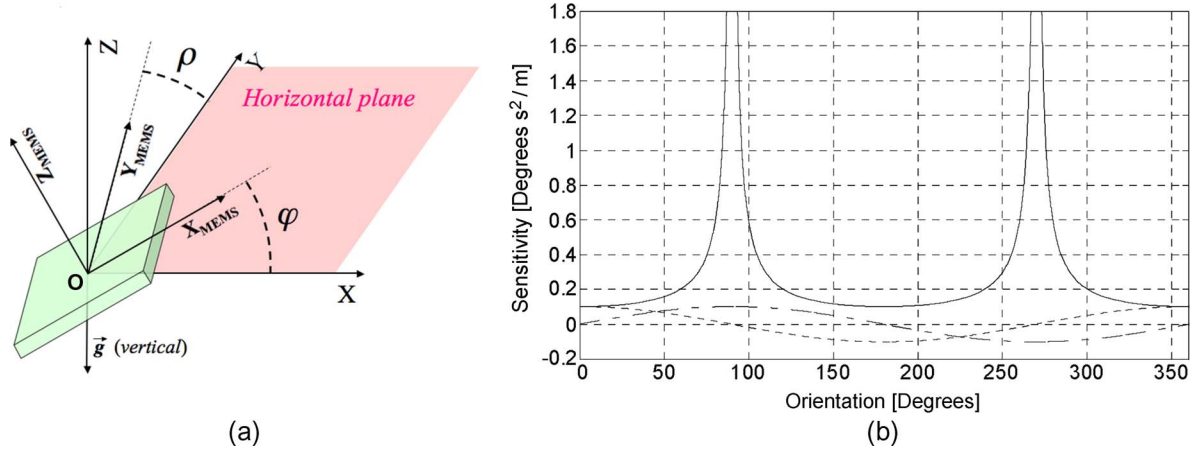
Fig. 1. (a) Angles φ and ρ that describe the orientation of the MEMS accelerometer with respect to an absolute reference system having the Z-axis oriented parallel to the gravity vector. The local reference system is indicated as $[0\ X_{\text{MEMS}}, Y_{\text{MEMS}}, Z_{\text{MEMS}}]$. (b) Sensitivity for the acceleration is computed. The continuous line refers to (9) and expresses the sensitivity of φ with respect to a_x. The dotted and dashed lines refer to (10). The first expresses the sensitivity of φ with respect to a_x and the second as a function of a_z. For simplicity, these two functions are computed for $a_y = 0$.

TABLE I
SOME OF THE MOST SIGNIFICANT PARAMETERS OF THE
LIS3L02AL MEMS ACCELEROMETER

Parameter	Value	Unit
Zero-g level	$V_{cc}/2 \pm 6\%$	V
Bias drift vs. temperature	$\pm 1.47 \cdot 10^{-2}$	m / (s^2·°C)
Acceleration range	± 20	m/s^2
Sensitivity	$V_{cc}/49 \pm 10\%$	V / (m/s^2)
Cross-axis	± 2	% of sensitivity
Acceleration noise density	$5 \cdot 10^{-4}$	m / (s^2·√Hz)

B. Autocalibration

The autocalibration procedure is based on the fact that the modulus of the acceleration, in static conditions, is equal to that of the gravity acceleration g, that is

$$\sqrt{a_x^2 + a_y^2 + a_z^2} = g. \tag{3}$$

To compute the model parameters, we placed the sensor in N different random orientations. For each orientation, we evaluated the sensor output while maintaining it in a strictly static condition. We define an error e_k equal to the squared difference between the modulus of the acceleration output by the MEMS and g for the kth orientation as

$$e_k = a_x^2 + a_y^2 + a_z^2 - g^2$$
$$= \sum_{i=x,y,z} \left\{ \sum_{j=(x,y,z)} [S_{ij} \cdot (V_{j,k} - O_j)]^2 \right\} - g^2 \tag{4}$$

where $V_{j,k}$ is the jth MEMS output for the kth orientation.

By adding e_k^2's over all the measured orientations, a cumulative error E is obtained as

$$E = E(O_x, O_y, O_z, S_{xx}, S_{yy}, S_{zz}, S_{xy}, S_{xz}, S_{yz}) = \frac{\sum\limits_{k=1}^{N} e_k^2}{N} \tag{5}$$

which is a nonlinear function of the sensor parameters **S** and **O**. The parameters, which best fit the observation data in the least-squares sense, can be determined by minimizing the cumulative error E with respect to the parameters. To the scope, we have adopted Newton's method, which is an iterative optimization procedure that guarantees quadratic convergence [14]. Starting from an initial guess of the sensor parameters, which is the one provided by the sensor manufacturer, the solution is iteratively updated as

$$\mathbf{x}^{t+1} = \mathbf{x}^t - \alpha \cdot \mathbf{H}^{-1}(\mathbf{x}^t) \cdot \mathbf{J}(\mathbf{x}^t) \tag{6}$$

where $\mathbf{x}^t$ is the unknown vector at the tth iteration, containing the bias vector and the six independent elements of the scale factor matrix: $x^t = [x_1, \ldots, x_9] = [O_x, O_y, O_z, S_{xx}, S_{yy}, S_{zz}, S_{xy}, S_{xz}, S_{yz}]^t$. $\mathbf{J}(\mathbf{x}^t)$ and $\mathbf{H}(\mathbf{x}^t)$ are the Jacobian vector and the Hessian matrix of the error E, respectively, defined as follows:

$$\mathbf{J}(\mathbf{x}^t) = \left[\frac{\partial E}{\partial x_1}, \ldots, \frac{\partial E}{\partial x_9} \right], \qquad \mathbf{H}(\mathbf{x}^t) = \left\{ h_{ij} = \frac{\partial^2 E}{\partial x_i \partial x_j} \right\}. \tag{7}$$

α is a damping parameter smaller than 1 and is computed at each iteration by means of a line search procedure [14]. Iterations are stopped when the following convergence criterion is satisfied:

$$\max \left\{ \left| \frac{x_l^t - x_l^{t-1}}{(x_l^t + x_l^{t-1})/2} \right| \right\} < \varepsilon \tag{8}$$

where ε is a threshold, which has empirically been set equal to $1.5 \cdot 10^{-6}$. Less than ten iterations are generally sufficient to converge. The accuracy on the parameter estimate can be assessed through the covariance analysis [15] carried out on the linearized version of (4) and (5) around the final value of the parameters. The results of this analysis are reported in Table II.

TABLE II
PARAMETERS ESTIMATED WITH THE CLASSICAL SIX-PARAMETER MODEL [5] (CALIB I) AND THE NINE-PARAMETER MODEL
INTRODUCED HERE (CALIB II). EACH PARAMETER IS REPORTED ALONG WITH ITS STANDARD DEVIATION

MEMS ID		Bias parameters		
		O_X	O_Y	O_Z
	Factory	0.5	0.5	0.5
#1	Calib I	$0.4910 \pm 3.2\cdot10^{-4}$	$0.4872 \pm 6.3\cdot10^{-4}$	$0.5485 \pm 3.6\cdot10^{-4}$
(N = 72)	Calib II	$0.49 \pm 1.0\cdot10^{-2}$	$0.486 \pm 9.2\cdot10^{-3}$	$0.55 \pm 1.3\cdot10^{-2}$
#2	Calib I	$0.5193 \pm 1.8\cdot10^{-4}$	$0.4988 \pm 6.2\cdot10^{-4}$	$0.5105 \pm 2.2\cdot10^{-4}$
(N = 42)	Calib II	$0.520 \pm 4.0\cdot10^{-3}$	$0.500 \pm 2.7\cdot10^{-3}$	$0.000 \pm 5.9\cdot10^{-3}$
#3	Calib I	$0.429 \pm 4.2\cdot10^{-3}$	$0.492 \pm 1.2\cdot10^{-3}$	$0.497 \pm 1.1\cdot10^{-3}$
(N = 35)	Calib II	$0.42 \pm 7.1\cdot10^{-2}$	$0.49 \pm 3.6\cdot10^{-2}$	$0.49 \pm 2.7\cdot10^{-2}$
#4	Calib I	$0.448 \pm 1.4\cdot10^{-3}$	$0.5229 \pm 3.2\cdot10^{-4}$	$0.4536 \pm 2.8\cdot10^{-4}$
(N = 35)	Calib II	$0.45 \pm 1.2\cdot10^{-2}$	$0.520 \pm 5.9\cdot10^{-3}$	$0.453 \pm 4.2\cdot10^{-3}$

MEMS ID		Scale factor		
		S_X	S_Y	S_Z
	Factory	5.0	5.0	5.0
#1	Calib I	$5.09 \pm 1.3\cdot10^{-2}$	$5.10 \pm 2.0\cdot10^{-2}$	$5.25 \pm 1.3\cdot10^{-2}$
(N = 72)	Calib II	$5.09 \pm 1.1\cdot10^{-2}$	$5.14 \pm 3.0\cdot10^{-2}$	$5.23 \pm 1.0\cdot10^{-2}$
#2	Calib I	$5.028 \pm 5.9\cdot10^{-3}$	$5.22 \pm 2.3\cdot10^{-2}$	$5.063 \pm 7.7\cdot10^{-3}$
(N = 42)	Calib II	$5.034 \pm 3.4\cdot10^{-3}$	$5.15 \pm 1.3\cdot10^{-2}$	$5.045 \pm 4.6\cdot10^{-3}$
#3	Calib I	5.6 ± 0.17	$5.64 \pm 5.6\cdot10^{-2}$	$4.94 \pm 3.9\cdot10^{-2}$
(N = 35)	Calib II	5.4 ± 0.21	$5.50 \pm 8.0\cdot10^{-2}$	$4.92 \pm 3.8\cdot10^{-2}$
#4	Calib I	$5.06 \pm 4.3\cdot10^{-2}$	$5.22 \pm 1.3\cdot10^{-2}$	$4.77 \pm 1.1\cdot10^{-2}$
(N = 35)	Calib II	$5.22 \pm 3.7\cdot10^{-2}$	$5.29 \pm 1.2\cdot10^{-2}$	$4.804 \pm 7.0\cdot10^{-3}$

MEMS ID		Cross-axis Scale factor		
		S_{XY}	S_{XZ}	S_{YZ}
#1	Calib II	$-0.0395 \pm 3.6\cdot10^{-4}$	$0.0227 \pm 8.0\cdot10^{-4}$	$0.0020 \pm 4.2\cdot10^{-4}$
#2	Calib II	$-0.0431 \pm 1.4\cdot10^{-4}$	$-0.0041 \pm 4.0\cdot10^{-4}$	$-0.0205 \pm 2.1\cdot10^{-4}$
#3	Calib II	$0.128 \pm 6.3\cdot10^{-3}$	$0.147 \pm 3.0\cdot10^{-3}$	$0.060 \pm 1.4\cdot10^{-3}$
#4	Calib II	$-0.059 \pm 1.2\cdot10^{-3}$	$-0.0363 \pm 4.6\cdot10^{-4}$	$-0.0251 \pm 2.4\cdot10^{-4}$

The adoption of a least-squares method for finding the solution of the calibration problem is based on the assumption that the noise affecting the measured data is additive and zero mean. The output of a MEMS is mainly affected by the thermal and electronic noise [11], [13], which are usually modeled as additive white Gaussian noise (AWGN) added to the analogic output of each sensor channel. These signals are then sampled and quantized, introducing a quantization noise characterized by zero-mean uniform probability density and white power spectral density. It can, therefore, be assumed that the output of the MEMS is corrupted by an unbiased additive white noise that is statistically independent from the signal. Consequently, by averaging many samples of the MEMS output for a sufficiently long time, the standard deviation of this noise can largely be reduced. This is sufficient when considering the optimal estimate of the model parameters, which minimizes the error E in a least-square sense.

C. Orientation Computation

Once the autocalibration procedure has been completed, the accelerometer is ready to be used. We first observe that the orientation of MEMS in 3-D space can be defined by only two angles, which represent the orientation of the device with respect to the gravity vector **g**; the rotation around an axis parallel to **g** cannot be observed since the sensor output is invariant for rotations around such an axis.

Fig. 2. Orientation of the MEMS accelerometer expressed both with the orientation angles (ϕ and ρ) and with the Euler angles (α, β, γ). Because the value of α is irrelevant, it is arbitrarily set to 0; consequently, the nodes' axis N coincides with the X-axis.

Let us define an absolute reference frame having the Z-axis parallel to **g**. Let us indicate as (φ, ρ) the angles between the X_{MEMS} and Y_{MEMS} axes and the horizontal plane [Fig. 1(a)]. From the acceleration vector obtained through (1), the angles φ and ρ could be computed by means of the following equations:

$$\varphi = \arcsin(a_x), \qquad \rho = \arcsin(a_y). \qquad (9)$$

The equations in (9) are frequently used with biaxial accelerometers, but they suffer from a critical drawback: The sensitivity on the estimated value of φ and ρ depends on the value of φ and ρ itself, as shown in Fig. 1(b). To overcome this
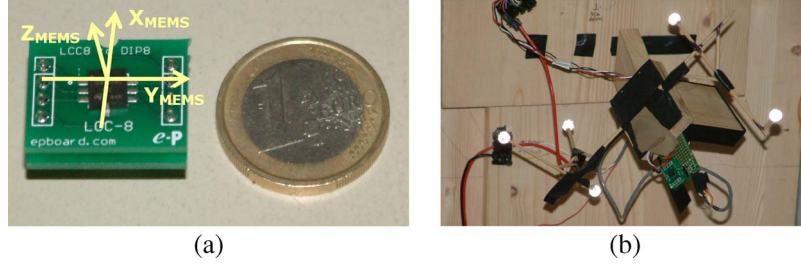
Fig. 3. (a) Zoom of the MEMS mounted on a board is shown along with the MEMS local reference system set by the manufacturer. (b) Structure on which the MEMS is attached is shown with five markers rigidly connected to the MEMS sensor.

problem, the following trigonometric equations are used here to compute φ and ρ:

$$\varphi = \arctan\left(\frac{a_x}{\sqrt{a_y^2 + a_z^2}}\right), \qquad \rho = \arctan\left(\frac{a_y}{\sqrt{a_x^2 + a_z^2}}\right). \tag{10}$$

These equations guarantee that the accuracy is almost constant inside the whole range of values that φ and ρ can assume, as shown by the dotted and dashed lines in Fig. 1(b).

The two angles defined in (10) represent two independent orientation parameters in the sense that any error on the estimate of φ does not influence the estimate on ρ and *vice versa*. Another possible angles system used to describe orientation is through Euler angles. These do not enjoy the same property of (φ, ρ) angles because they are defined as a sequence of rotations (cf. Fig. 2 and the Appendix).

To express the sensor orientation in terms of the Euler angles (α, β, γ), we have derived the relationship between (φ, ρ) and (α, β, γ), which is reported in the Appendix [see (A3) and (A8)]. The following relationships are obtained:

$$\alpha = 0$$
$$\sin(\beta) = \sqrt{\sin^2(\varphi) + \sin^2(\rho)}, \qquad (0 \le \beta \le \pi)$$
$$\sin(\gamma) = \frac{\sin(\varphi)}{\sin(\beta)} = \frac{\sin(\varphi)}{\sqrt{\sin^2(\varphi) + \sin^2(\rho)}}. \tag{11}$$

Since the angle α expresses a rotation around the absolute vertical axis, it cannot be measured by MEMS. It remains undetermined, and it can be set equal to zero.

III. RESULTS

The proposed calibration procedure has been applied to four MEMS accelerometers produced by ST Microelectronics (model LIS3L02AL) [10]. They are triaxial linear analogic accelerometers that are capable of measuring accelerations in the range $[-2g, +2g]$ along each axis. The typical bias and scale parameter, as provided by the manufacturer, are reported in Table I. If a normalized voltage is considered, the typical value of the parameters is 0.5 and 5 m/s^2, respectively.

The output of the MEMS accelerometers is acquired by a host computer at a rate of 960 Hz through a NI-DAQ board. An analog low-pass RC filter has been added to the accelerometer output to filter high-frequency noise and avoid aliasing, which would have been introduced by sampling. The bandwidth of the filter was set to 285 Hz, which is large enough for the human finest-motion frequency content [16].

To evaluate the accuracy of the autocalibration procedure, we have compared the orientation angles computed in (10) with the same angles computed by a commercial motion capture system, that is, the SMART3D [17]. This system is able to compute the 3-D position of a set of retroreflective markers whose position is surveyed by six cameras. The working volume of the motion capture system was approximately 500 mm $\times$ 500 mm $\times$ 500 mm, which allowed accommodating different MEMS orientations with optimal marker visibility. With this working volume, the markers are localized with an accuracy of 0.1 mm (RMS error).

The markers and accelerometer, which are rigidly connected to each other, were fixed on a frame that could be oriented in any direction, as shown in Fig. 3(b). Five markers were located the vicinity of the accelerometer. The orientation of the MEMS supporting structure is then computed as the mean rotational component of the rigid motion undergone by the markers. The angular accuracy in the measurement of this orientation can be derived from the spatial accuracy in the localization of the markers. This can be done by determining the sensitivity of the angular displacement with respect to a spatial displacement, as described in [18]. For the adopted setup (five markers, spatial accuracy of 0.1 mm (RMS) and minimum distance of 100 mm from the accelerometer), the angular accuracy in the measurement of the orientation of the MEMS results in being better than 0.025° (RMS).

The vertical direction of the motion capture reference system was carefully established to guarantee that it is parallel to gravity by surveying two markers put onto the wire of a plumb line held along the vertical.

From the 3-D position of the five markers positioned on the MEMS board, we computed the angles φ and ρ, which define the orientation of the structure and consequently of the MEMS accelerometer in the motion capture reference system. This has been done by using quaternions [20] that allow determining the rotation by solving a linear system, thereby guaranteeing the orthonormality of the obtained rotation matrix. At the same time, for each sampled orientation, the angles φ and ρ are also estimated by processing the MEMS sensor output through (10).

The high accuracy of the motion capture system lets us take its orientation measurements as the ground truth. For this

TABLE III
MEAN ERROR AND STANDARD DEVIATION OF THE MEASURED ORIENTATION, EXPRESSED BY ANGLES φ AND ρ (FIRST TWO BLOCKS) AND WITH THE EULER ANGLES β AND γ (SECOND TWO BLOCKS), FOR THE FOUR ACCELEROMETERS CALIBRATED WITH THE FACTORY CALIBRATION DATA (COLUMN FACTORY), WITH THE CLASSICAL SIX-PARAMETER MODEL REPORTED IN [11] (COLUMN CALIB I) AND THE NOVEL NINE-PARAMETER MODEL INTRODUCED HERE (COLUMN CALIB II). ERRORS ARE IN DEGREES

MEMS device	# samples (N)	φ: mean error ± std.dev. [degrees]		
		Factory	Calib I	Calib II
#1	72	-2.23 ± 6.84	$+0.24 \pm 0.53$	$+0.18 \pm 0.47$
#2	42	$+3.38 \pm 2.77$	$+0.15 \pm 0.60$	-0.21 ± 0.59
#3	35	-23.10 ± 3.37	-1.54 ± 1.81	-0.26 ± 1.44
#4	35	-14.90 ± 4.86	$+0.58 \pm 0.91$	-0.20 ± 0.74
MEMS device	# samples (N)	ρ: mean error ± std.dev. [degrees]		
		Factory	Calib I	Calib II
#1	72	-0.05 ± 6.40	-0.09 ± 0.65	$+0.11 \pm 0.59$
#2	42	$+0.80 \pm 2.52$	$+0.41 \pm 0.51$	$+0.03 \pm 0.34$
#3	35	$+0.77 \pm 10.38$	$+1.15 \pm 1.66$	$+0.26 \pm 1.11$
#4	35	$+6.15 \pm 8.12$	-0.42 ± 0.68	$+0.00 \pm 0.50$
MEMS device	# samples (N)	β: mean error ± std.dev. [degrees]		
		Factory	Calib I	Calib II
#1	72	$+1.47 \pm 11.17$	-0.01 ± 0.59	$+0.11 \pm 0.59$
#2	42	-0.34 ± 3.18	-0.09 ± 0.56	$+0.03 \pm 0.56$
#3	35	-8.34 ± 10.73	-0.57 ± 1.34	-0.31 ± 1.11
#4	35	-8.62 ± 12.60	$+0.31 \pm 0.56$	-0.03 ± 0.47
MEMS device	# samples (N)	γ: mean error ± std.dev. [degrees]		
		Factory	Calib I	Calib II
#1	72	-1.99 ± 4.37	$+0.31 \pm 1.02$	$+0.23 \pm 0.81$
#2	42	$+5.28 \pm 7.22$	$+0.24 \pm 0.61$	-0.10 ± 0.37
#3	35	-27.11 ± 13.38	-0.94 ± 6.48	-0.46 ± 1.76
#4	35	-18.81 ± 22.34	$+0.99 \pm 1.81$	-0.12 ± 0.45

reason, we adopted a comparative approach to evaluate the accuracy of the orientation angles φ and ρ, comparing the value output by the MEMS with those computed through the motion-capture system data.

The mean estimated value of the biases and the scale factors ± their standard deviation obtained by using the six- and nine-parameter model introduced here are reported in Table II, in the rows indicated with "Calib I" and "Calib II," respectively. N represents the number of random orientations acquired for each accelerometer. The residuals, i.e., E in (5), for the four accelerometers were, respectively, 0.0151, 0.0069, 0.0365, and 0.0085 for Calib I and 0.0117, 0.0032, 0.0263, and 0.0039 for Calib II. As can be appreciated, the estimate uncertainty is below 0.5% and is often much lower. In particular, the uncertainty on the scale factor consistently improves when the nine-parameter model is adopted.

The estimated orientation angles along with their standard deviation are reported in Table III, which describes the metrological performance of the sensor in the attitude estimate.

The error in the angle estimate ranges from $-23.10°$ to $+6.15°$ when factory calibration data are used. It decreases to the range $-1.54°$ to $+1.15°$ when the six-parameter model was used in (1), and it further decreases to the range $-0.26°$ to $+0.26°$ when the nine-parameter model was adopted.

To investigate the spatial distribution of the errors, we define the error angles $\Delta\varphi$ and $\Delta\rho$ as

$$\begin{cases} \Delta\varphi = \varphi_{\text{MEMS}} - \varphi_{\text{SMART3D}} \\ \Delta\rho = \rho_{\text{MEMS}} - \rho_{\text{SMART3D}} \end{cases} \quad (12)$$

and plot them in Fig. 4 for one of the sensors (sensor #1). As can be seen, errors do not show any particular space dependence. By using factory calibration data [Fig. 4(a)], errors are distributed approximately inside a circle centered in [0, 0]. The dimension of this circle is greatly reduced when autocalibration is carried out and, in particular, when the nine-parameter model is adopted [Fig. 4(b)]. Fig. 4(c) and (d) show that, thanks to the particular trigonometric formulation of (10), the error is isotropic, as it does not depend on the values assumed by φ and ρ. Similar results are obtained for the other accelerometers calibrated.

IV. DISCUSSION

MEMS calibration is usually carried out in the factory. A dedicated machine positions a MEMS accelerometer in several precisely known orientations. It reads the MEMS output and estimates the diagonal parameters of the scale factor
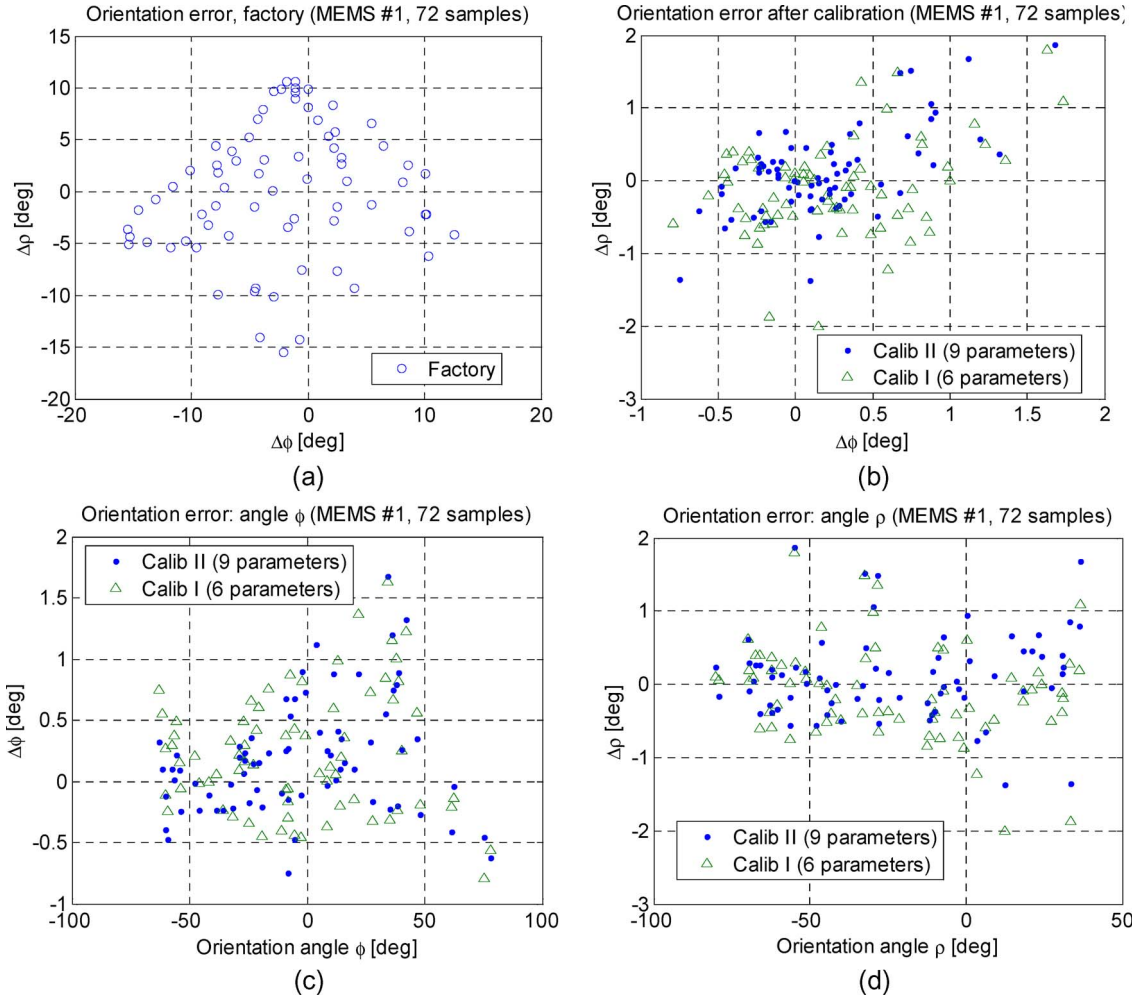
Fig. 4. Error in the estimate of φ and ρ for the 72 orientations measured for sensor #1.

matrix S $[S_x, S_y, S_z]$ and the three bias values $[O_x, O_y, O_z]$. This procedure is quite time consuming for large MEMS production and not very effective as these parameters may change when MEMS are placed in the operating environment, because of their sensitivity to temperature.

To avoid these drawbacks, autocalibration has recently been introduced with a six-parameter model [11], leading to a significant improvement with respect to using factory calibration data. The results reported in Table III ("Calib I" column) show a residual error on the order of a few degrees on the orientation measurements, whereas the measurement error was as large as $20°$ with factory calibration data (MEMS #3 in Table III). However, the accuracy can further be improved by also considering the cross-axis terms inside the scale factor matrix, leading to the nine-parameter model proposed here ("Calib II" column of Table III). With this model, the accuracy is reduced to less than one degree ($\pm 0.26°$). The improvement with respect to the classical six-parameter model is, therefore, almost one order of magnitude and is consistent in all the calibration experiments.

This fact, together with the very low uncertainty in the parameter estimate (cf. Table II), can reasonably be interpreted as a better model-fitting capability of the proposed nine-parameter model with respect to the six-parameter model. This allows us to draw the conclusion that the three cross-axis scale parameters

in the present model allow a better fitting of the physical MEMS behavior.

The value of scale parameters and biases obtained through autocalibration is generally close but not equal to that provided by the manufacturer. The typical differences are on the order of $\pm 10\%$ for the bias and $\pm 5\%$ for the scale factor (cf. Table II). However, when they are used to compute the MEMS orientation, this error is amplified. The error was in some cases larger than $20°$ (MEMS #3 in Table II), with standard deviation exceeding $10°$, when the values of $\mathbf{S}$ and $\mathbf{O}$ given by the factory (and null cross-axis scale factors) were used. Nevertheless, factory parameters can be used as a reliable initialization point for Newton's optimization, and a small number of iterations are sufficient to obtain a reliable and accurate estimate of the sensor parameters.

The symmetrical matrix $\mathbf{S}$ considered here can take into account the crosstalk between axes. This is the electric coupling between pairs of output channels, which usually produces a symmetrical effect [13], [20]. It can also accommodate symmetrical axis misalignment, which can be described by what is called a *geometrical deformation* [14, Fig. 5(a)].

Other parameters, that is, the anti-symmetric components, could be accommodated inside the matrix $\mathbf{S}$. However, they would lead to overfitting, as we have experimentally verified
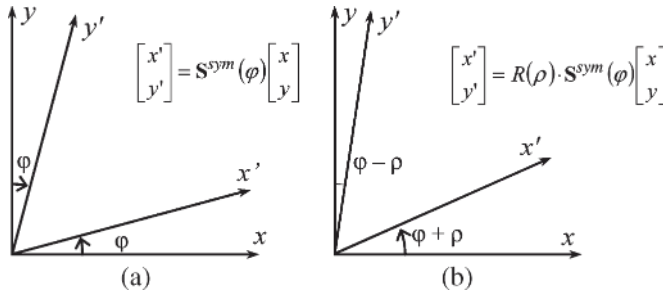
Fig. 5. Two-dimensional pictorial representation of two types of axis misalignment (adapted from [14, Fig. 2.7]). (a) *Geometrical deformation*. The two axes are rotated by an angle of the same amplitude but opposite sign. In this case, the transformation can be expressed by a symmetrical matrix $\mathbf{S^{sym}}(\varphi)$. (b) Deformation followed by a rotation. In this case, the angle between the two axes, after the transformation, is the same as in (a), but they are both rotated by the same amount ρ. In this case, the transformation is described by a nonsymmetrical matrix, resulting from the product of the rotation matrix $\mathbf{R}(\rho)$ and the same deformation matrix $\mathbf{S^{sym}}(\varphi)$ of (a).

that the accuracy of the sensor decreases in this case. For this reason, a symmetrical scale factor matrix $\mathbf{S^{sym}}$ has been considered in (1).

In the general case, however, axis misalignment is not symmetrical [cf. Fig. 5(b)], and it is described by the product of a rotation matrix $\mathbf{R}$ and a symmetrical deformation matrix $\mathbf{S^{sym}}$ [21], i.e.,

$$\mathbf{S^{asym}} = \mathbf{R} \cdot \mathbf{S^{sym}} \tag{13}$$

where $\mathbf{S^{sym}}$ is the symmetrical scale factor matrix used in our model.

To understand the role $\mathbf{R}$, we have to recall that the actual orientation of the MEMS sensing axes $[0 \; X_{\mathrm{sens}}, Y_{\mathrm{sens}}, Z_{\mathrm{sens}}]$ is implicitly established at calibration time. In fact, minimizing (5), when MEMS is horizontal, the sensing axes are oriented such that the sum of the angles between Z_{sens} and the gravity acceleration, and between X_{sens} and Y_{sens} and the horizontal plane, is minimum in the l^2 norm. Any residual rotation between sensing axes and the local reference system, which specifies the MEMS case orientation in space $[[0 \; X_{\mathrm{MEMS}}, Y_{\mathrm{MEMS}}, Z_{\mathrm{MEMS}}]$ in Fig. 1(a)], is represented by the matrix $\mathbf{R}$. This rotation cannot be recovered by any autocalibration method, as it would require that the MEMS absolute orientation is exactly known in all the calibration positions, which cannot be done inside an autocalibration procedure. However, it should be remarked that the residual error after calibration, by using only a symmetrical scale factor matrix $\mathbf{S^{sym}}$, is extremely low (cf. Table III, column "Calib II"). Therefore, the type of axis misalignment, which can be expressed as a pure rotation, can be considered as having a little impact on the MEMS accuracy.

V. CONCLUSION

In this paper, we have presented an on-the-field autocalibration procedure for MEMS triaxial accelerometers, which requires neither any equipment nor a controlled environment. It computes the sensor bias and scale factor based on a novel nine-parameter model, which also incorporates cross-axis scale factors. This has allowed increasing, almost one order of mag-

nitude, the accuracy with respect to the classical autocalibration models presented in the literature. A new and reliable procedure to evaluate the calibration performance, based on a motion capture system, has also been presented.

APPENDIX
RELATIONSHIP BETWEEN TILT (φ, ρ) AND EULER ANGLES (α, β, γ)

The Euler angles considered here measure three sequential (not independent) rotations of the local reference system $[O \; X_{\mathrm{MEMS}} \; Y_{\mathrm{MEMS}} \; Z_{\mathrm{MEMS}}]$ with respect to the absolute reference one $[O \; X \; Y \; Z]$. They are defined as follows. The angle α measures the rotation around the absolute vertical axis Z. The angle β measures the rotation around the node axis N, that is, the X-axis after rotating around Z. Finally, the angle γ measures the rotation around the local Z-axis Z_{MEMS}. In this particular case, α cannot be determined as the rotation of MEMS around the absolute vertical axis cannot be appreciated. For this reason, in the following, $\alpha = 0$ will be assumed and the node axis is coincident with the X-axis.

Defining $(\mathbf{u_X}, \mathbf{u_Y}, \mathbf{u_Z})$ as the three versors in the absolute frame and $(\mathbf{x_S}, \mathbf{y_S}, \mathbf{z_S})$ as the versors of the sensor's frame, we can express the orientation angles through the inner product $\langle . \rangle$ as follows:

$$\begin{aligned} \cos(\beta) &= \langle \mathbf{z_S}, \mathbf{u_Z} \rangle, & \sin(\varphi) &= \langle \mathbf{x_S}, \mathbf{u_Z} \rangle \\ \cos(\gamma) &= \langle \mathbf{x_S}, \mathbf{u_X} \rangle, & \sin(\rho) &= \langle \mathbf{y_S}, \mathbf{u_Z} \rangle. \end{aligned} \tag{A1}$$

By imposing the unitary norm of the versor $\mathbf{u_Z}$, we obtain

$$\begin{aligned} \|\mathbf{u_Z}\|^2 &= \langle \mathbf{x_S}, \mathbf{u_Z} \rangle^2 + \langle \mathbf{y_S}, \mathbf{u_Z} \rangle^2 + \langle \mathbf{z_S}, \mathbf{u_Z} \rangle^2 \\ &= \sin^2(\varphi) + \sin^2(\rho) + \cos^2(\beta) = 1. \end{aligned} \tag{A2}$$

Isolating β in the preceding equation, we obtain

$$\sin^2(\varphi) + \sin^2(\rho) = 1 - \cos^2(\beta) = \sin^2(\beta). \tag{A3}$$

Considering that $\sin(\beta) \geq 0$ because, in the Euler convention, $0 \leq \beta \leq \pi$, β can be derived from the tilt angles as follows:

$$\sin(\beta) = \sqrt{\sin^2(\varphi) + \sin^2(\rho)}, \qquad (0 \leq \beta < \pi). \tag{A4}$$

As far as γ is concerned, let us consider the projection on the XY plane of the unit circle on the plane $x_S y_S$, which is represented in Fig. 6. The projection of this circle forms an ellipse of axes OA_X and OA_Y, where $\overline{OA_X} = 1$, and $\overline{OA_Y} = \cos(\beta)$. The vector $\overline{OS}$, that is, the projection of the versor $\mathbf{x_S}$ on the plane XY, has the components

$$\|\overline{OB}\| = (\mathbf{x_S}, \mathbf{u_X}) = \cos(\gamma)$$
$$\|\overline{OC}\| = (\mathbf{x_S}, \mathbf{u_Y}) = \sin(\gamma)\cos(\beta). \tag{A5}$$

On the other hand, φ is defined as the angle between $\mathbf{x_S}$ and $\overline{OS}$; therefore, $\|\overline{OS}\| = \cos(\varphi)$.

By imposing $\|\overline{OS}\|^2 = \|\overline{OB}\|^2 + \|\overline{OC}\|^2$, we obtain

$$\cos^2(\varphi) = \cos^2(\gamma) + \sin^2(\gamma)\cos^2(\beta). \tag{A6}$$

Fig. 6. Unit circle defined by the versors $\mathbf{x_S}$ and $\mathbf{y_S}$ projected on the XY plane.

A manipulation of (A5) gives

$$
\begin{aligned}
\sin^2(\varphi) &= \sin^2(\gamma) - \sin^2(\gamma)\cos^2(\beta) \\
&= \sin^2(\gamma)\left(1 - \cos^2(\beta)\right) \\
&= \sin^2(\gamma)\sin^2(\beta).
\end{aligned} \tag{A7}
$$

Assuming that $\varphi \geq 0$ for $0 \leq \gamma \leq \pi$, as shown in Fig. 6, and considering that $\sin(\beta) \geq 0$, γ can be computed as

$$
\sin(\gamma) = \frac{\sin(\varphi)}{\sin(\beta)} = \frac{\sin(\varphi)}{\sqrt{\sin^2(\varphi) + \sin^2(\rho)}}. \tag{A8}
$$

REFERENCES

[1] J. K. Perng, B. Fischer, S. Hollar, and K. S. J. Pister, "Acceleration sensing glove (ASG)," in *Proc. ISWC*, 1999, pp. 178–180.

[2] M. S. Conover, "Using accelerometers to quantify infant general movements as a tool for assessing motility to assist in making diagnosis of cerebral palsy," M.S. thesis, Virginia Polytech. Inst. State Univ., Blacksburg, VA, 2003.

[3] R. Barbieri, E. Farella, L. Benini, B. Ricco, and A. Acquiaviva, "A low power motion capture system with integrated accelerometers," in *Proc. CCNC*, 2004, pp. 418–423.

[4] D. Giansanti, G. Maccioni, and V. Macellari, "The development and test of a device for the reconstruction of 3-D position and orientation by means of a kinematic sensor assembly with rate gyroscopes and accelerometers," *IEEE Trans. Biomed. Eng.*, vol. 52, no. 7, pp. 1271–1277, Jul. 2005.

[5] D. Roetenberg, P. J. Slycke, and P. H. Veltink, "Ambulatory position and orientation tracking fusing magnetic and inertial sensing," *IEEE Trans. Biomed. Eng.*, vol. 54, no. 5, pp. 883–890, May 2007.

[6] C. W. Tan and S. Park, "Design of accelerometer-based inertial navigation systems," *IEEE Trans. Instrum. Meas.*, vol. 54, no. 6, pp. 2520–2530, Dec. 2005.

[7] T. Sakaguchi, T. Kanamori, and H. Katayose, "Human motion capture by integrating gyroscopes and accelerometers," in *Proc. IEEE/SICE/RSJ MFI*, 1996, pp. 470–475.

[8] S. Kurata, M. Makikawa, H. Kobayashi, A. Takahashi, and R. Tokue, "Joint motion monitoring by accelerometers set at both near sides around the joint," in *Proc. IEEE EMBC*, 1998, pp. 1936–1939.

[9] A. Krohn, M. Beigl, C. Decker, U. Kochendörfer, P. Robinson, and T. Zimmer, "Inexpensive and automatic calibration for acceleration sensors," in *Proc. UCS*, 2004, pp. 245–258.

[10] STMicroelectronics, *LIS3L02AL 3axis-2g linear accelerometer*, 2004. [Online]. Available: http://www.st.com/stonline/

[11] Z. C. Wu, Z. F. Wang, and Y. Ge, "Gravity based online calibration for monolithic triaxial accelerometers' gain and offset drift," in *Proc. 4th World Congr. Intell. Control Autom.*, 2002, pp. 2171–2175.

[12] N. Yazdi, F. Ayazi, and K. Najafi, "Micromachined inertial sensors," *Proc. IEEE*, vol. 86, no. 8, pp. 1640–1659, Aug. 1998.

[13] T. Mineta, S. Kobayashi, Y. Watanabe, S. Kanauchi, I. Nakagawa, E. Suganurna, and M. Esashi, "Three-axis capacitive accelerometer with uniform axial sensitivities," in *Proc. Solid-State Sens. Actuators, Eurosensors IX. Transducers*, 1995, vol. 2, pp. 554–557.

[14] K. Madsen, H. B. Nielsen, and O. Tingleff, *Methods for Non-Linear Least Squares Problems*, 2nd ed. Lyngby, Denmark: IMM, Tech. Univ. Denmark, 2004.

[15] W. H. Press, S. A. Teukolsky, W. T. Vetterling, and B. P. Flannery, *Numerical Recipes 3rd Edition: The Art of Scientific Computing*. Cambridge, U.K.: Cambridge Univ. Press, 2003.

[16] D. Winter, *Biomechanics and Motor Control of Human Movement*. Hoboken, NJ: Wiley, 1990.

[17] [Online]. Available: http://www.bts.it

[18] N. C. Barford, *Experimental Measurements: Precision, Error and Truth*. Hoboken, NJ: Wiley, 1985.

[19] O. Faugeras, *Three-Dimensional Computer Vision*. Cambridge, MA: MIT Press, 1993.

[20] M. Alonso and E. J. Finn, *Fundamental University Physics*, vol. 2, Fields and Waves. Amsterdam, The Netherlands: Inter Eur., 1974.

[21] R. Hartley and A. Zisserman, *Multiple View Geometry in Computer Vision*, 2nd ed. Cambridge, U.K.: Cambridge Univ. Press, 2003.

Iuri Frosio (M'07) received the M.Sc. and Ph.D. degrees in biomedical engineering from Politecnico di Milano, Milan, Italy, in 2002 and 2006, respectively.

Since 2006, he has been an Assistant Professor with the Department of Computer Science, University of Milano. His research interests include medical image processing, virtual reality, artificial intelligence, and movement analysis.

Federico Pedersini received the "Laurea" (*cum laude*) and Ph.D. degrees in electronics and telecomunication engineering from Politecnico di Milano, Milan, Italy, in 1991 and 1994, respectively.

Until 2001, he was with the Department of Electrical Engineering, Politecnico di Milano, where he was doing research mainly in the field of image processing for 3-D reconstruction and camera calibration. Since 2003, he has been with the Department of Computer Science, University of Milano, where he has been an Associate Professor of digital architectures since 2005. His research interests include signal and image processing for measurement and analysis, as well as architectures and algorithms for wireless sensor networks.

N. Alberto Borghese (M'97) received the degree with full marks and honors from Politecnico di Milano, Milan, Italy, in 1985.

He was a Visiting Scholar with the Center for Neural Engineering, University of Southern California, Los Angeles, in 1991, with the Department of Electrical Engineering, California Institute of Technology, Pasadena, in 1992, and with the Department of Motion Capture of Electronic Arts, Vancouver, BC, Canada, in 2000. He is currently an Associate Professor with the Department of Computer Science, University of Milano, where he teaches courses on intelligent systems and robotics and is the Director of the Applied Intelligent Systems Laboratory. He has coauthored more than 40 peer-reviewed journal papers and is the holder of several patents. His research interests include quantitative human motion analysis and modeling, statistical learning from data, and applications to vision, graphics, and medical imaging.